

AFO SIRT R 97-0699

REPORT DOCUMENTATION PAGE			Form Approved OMB No. 0704-0188	
<small>Public reporting burden for this collection of information is estimated to average 1 hour per response, including the time for reviewing instructions, searching existing data sources, gathering and maintaining the data needed, and completing and reviewing the collection of information. Send comments regarding this burden estimate or any other aspect of this collection of information, including suggestions for reducing the burden, to Washington Headquarters Services, Directorate for Information Operations and Reports, 1215 Jefferson Davis Highway, Suite 1204, Arlington, VA 22202-4302, and to the Office of Management and Budget, Paperwork Reduction Project (0704-0188), Washington, DC 20503.</small>				
1. AGENCY USE ONLY (Leave blank)	2. REPORT DATE November 1997	3. REPORT TYPE AND DATES COVERED Final Report 01 Jul 94 - 30 Jun 97		
4. TITLE AND SUBTITLE Upper Mantle Structure in the Middle East, Central Asia, Lake Baikal and Far East from Pn Tomography and Sn Attenuation		5. FUNDING NUMBERS F49620-94-1-0310 DAO-DE AFDW/FS		
6. AUTHOR(S) Thomas Hearn, James Ni, Richard Rapine, Christopher Reese				
7. PERFORMING ORGANIZATION NAME(S) AND ADDRESS(ES) New Mexico State University Department of Physics Las Cruces, NM 88003-8001		8. PERFORMING ORGANIZATION REPORT NUMBER		
9. SPONSORING/MONITORING AGENCY NAME(S) AND ADDRESS(ES) AFOSR/NM 110 Duncan Ave., B115 Bolling AFB, DC 20332-8050		10. SPONSORING/MONITORING AGENCY REPORT NUMBER		
11. SUPPLEMENTARY NOTES This research was sponsored by AFOSR.				
12a. DISTRIBUTION/AVAILABILITY STATEMENT Approved for public release distribution unlimited.		12b. DISTRIBUTION CODE		
13. ABSTRACT (Maximum 200 words) We have studied the propagation efficiencies of the Sn and Lg phases throughout China and produced summary maps. In addition, estimates of coda Q, Q for the Pn phase, and Q for the Lg phase for Tibet have been made. Sn has difficulty propagating across extended terrains in eastern China, the northern Tibetan plateau, and Mongolia. This makes it a difficult phase to use for nuclear monitoring purposes. Analysis of the Pn and Lg Q for northern Tibet show that partial melt both in the uppermost mantle and middle crust quickly attenuate these phases. Lg does propagate well over most of the rest of China, especially when it does not traverse major changes in crustal structure.				
14. SUBJECT TERMS Seismic attenuation, wave propagation in the Middle East and southern Asia.		15. NUMBER OF PAGES 35		16. PRICE CODE
17. SECURITY CLASSIFICATION OF REPORT Unclassified	18. SECURITY CLASSIFICATION OF THIS PAGE Unclassified	19. SECURITY CLASSIFICATION OF ABSTRACT Unclassified	20. LIMITATION OF ABSTRACT SAR	

NSN 7540-01-280-5500

Standard Form 298 (Rev. 2-89)
Prescribed by ANSI Std. Z39-18
298-102

Commercial use is forbidden. Visit stone.abovetopsecret.com for more information on usage.

Final Technical Report, November 1997

**Uppermost Mantle Structure in the Middle East, Central Asia, Lake Baikal,
and Far East from Pn Tomography and Sn Attenuation**

Augmentation Award for Science and Engineering Research Training (AASERT)

Air Force Office of Scientific Research Contract No. F49620-94-1-0310

Contract Period: July 1, 1994 to June 1, 1997.

Principal Investigators: Thomas Hearn and James Ni.

New Mexico State University, Department of Physics, Las Cruces, NM, USA

Contents

Contents	1
List of Figures	2
Summary	3
Research accomplished	3
Background	3
Introduction	4
Regional Sn and Lg wave characteristics of western China	5
Attenuation of Coda waves in southern Tibet	6
Lateral variation of Pn propagation at the CDSN station LSA	8
Azimuthal variation of Q_{Lg} at the CDSN station LSA.	11
Conclusions	13
Acknowledgments	14
Figures	15
References	29
Publications resulting from this contract	31
Refereed publications	31
Conference proceedings	31
Abstracts and presentations	32
List of personnel involved with this contract	33

List of Figures

Figure 1: Tectonic map of China and surrounding regions	15
Figure 2: Map of seismic station and event locations	16
Figure 3: Map of efficient Sn propagation paths in China	17
Figure 4: Map of inefficient Sn propagation paths in China	18
Figure 5: Map of poor Sn propagation paths in China	19
Figure 6: Map of efficient Lg propagation paths in China	20
Figure 7: Map of inefficient Lg propagation paths in China	21
Figure 8: Map of poor Lg propagation paths in China	22
Figure 9: Summary map of Sn propagation in China	23
Figure 10: Summary map of Lg propagation in China	24
Figure 11: Station and event location map for Tibet	25
Figure 12: Comparison of coda Q for different regions	26
Figure 13: Map of Pn Q for Tibet from station LSA	27
Figure 14: Map of Lg Q for Tibet from station LSA	28

Summary

This report covers work done by NMSU graduate students Richard Rapine and Chris Reese during the time that they were supported by this ASSERT contract. Because of the need for nuclear test discriminants based upon regional phases, we have studied the propagation efficiencies of the Sn and Lg phases throughout China, and produced summary maps. In addition, estimates of coda Q, Q for the Pn phase, and Q for the Lg phase for Tibet have been made. Sn has difficulty propagating across extended terrains in eastern China, the northern Tibetan plateau, and Mongolia. This makes it a difficult phase to use for nuclear monitoring purposes. Analysis of the Pn and Lg Q for northern Tibet show that partial melt both in the uppermost mantle and middle crust quickly attenuate these phases. Southern Tibet has a more normal Q value. Lg does propagate well over most of the rest of China, especially when it does not traverse major changes in crustal structure.

Research Accomplished

Background

This Augmentation Award for Science and Engineering Research Training (AASERT) supported students working on our accompanying contract: Uppermost Mantle Structure in Southern Eurasia from Pn Tomography and Sn Attenuation (Hearn and Ni; AFOSR F49620-93-1-0429; 8/93 to 12/95). Some of the work has also been associated with a more recent DOE contract: Regional wave propagation characteristics in the Middle East and Southern Asia, (Ni and Hearn; Phillips Lab F19628-95-K-0009; 7/94 to 10/97). Under those contracts, we mapped the Pn propagation velocity for the Middle East, southern Europe, and southern Asia as well as the propagation efficiencies of the Sn and Lg phases for the Middle East. Final reports for both those contracts have been submitted and contain results that will only be summarized here. This report will concentrate primarily on the additional research accomplished by the two students supported under this AASERT contract: Richard Rapine and Chris Reese. Richard Rapine's work focused on mapping the extent of Sn and Lg propagation within China and its surrounding region, and Chris Reese's work utilized data from within Tibet to estimate attenuation for S-coda, Pn, and Lg.

More detailed discussions of this work can be found in the publications that have resulted from this contract and its companion contracts. The initial work that led to this contract was on the tomography of the Turkish Iranian Plateau [Hearn and Ni, 1994; Hearn and Ni, 1992a, b, c]. The tomography study of the Turkish-Iranian Plateau was followed by a study of Sn and Lg propagation efficiency for the region. This manuscript has also been presented and published [Rodgers, Ni, and

Hearn, 1997; Rodgers, Hearn and Ni, 1994a, b]. Estimates of Lg attenuation for the Turkish-Iranian Plateau were also published [Wu, Ni, and Hearn, 1995a, b].

Student work under this ASSERT has focused on China and surrounding regions. Mapping of Lg and Sn propagation in China and southern Asia by Richard Rapine has been presented and published [Rapine et al., 1995; Ni et al., 1995; Rapine, Ni, and Hearn, 1997]. Chris Reese made further estimates of seismic coda Q, Pn Q, and Lg Q for Tibet [Reese, Rapine, and Ni, 1997; Reese and Ni, 1996, Reese, Ni, and Hearn, 1995].

Introduction

Regional wave propagation studies have long been useful in problems associated with the proliferation of nuclear weapons. Regional studies serve a twofold purpose: (1) regional data can provide stable yield estimates for underground nuclear explosions, and (2) regional data can discriminate between explosions and earthquakes. For both of these goals, understanding the timing and strength of regional seismic phases is crucial. Regional seismic phases that are most useful in discrimination studies are the Pn, Sn, and Lg phases. Discriminants based on these types of regional data are generally not transportable and must be individually calibrated for a particular region.

Under our companion grants, we studied the characteristics of the Pn, Sn, and Lg seismic phases for southern Eurasia with an emphasis on the Middle East, southern Asia, and Tibet [Hearn and Ni, 1994; Hearn and Wu, 1995, 1998; Wu, Ni, and Hearn, 1996]. Regional variations of P-wave velocity and anisotropy in the uppermost mantle were found through the tomographic inversion of travel times and Sn and Lg propagation and attenuation were studied by a detailed examination of many thousands of raypaths for propagation efficiency. Pn tomography results indicate that much of the uppermost mantle beneath southern Eurasia has low P-wave velocity and a small amount of melt. Mapping of Sn propagation efficiency confirms that regions with low Pn velocity generally do not propagate Sn waves efficiently. This is especially true for the Turkish-Iranian Plateau and the northern Tibetan Plateau [Hearn & Ni, 1994; Rodgers, Ni, and Hearn, 1997]. In contrast to the Sn waves, Lg waves propagate within the crust and are insensitive to mantle properties, but are affected by changes in crustal structure. We found that Lg is weakened or completely absent when propagation paths obliquely cross major tectonic boundaries such as the Himalaya Mountains, the Tarim Basin, the Caucasus Mountains, or the oceanic crust of the Black and Caspian Seas [Rodgers, Ni, and Hearn, 1997]. Our work suggests that the high attenuation of Sn in many parts of southern Eurasia limits its use in regional nuclear monitoring; however, Lg can be observed provided

data is available from stations sited within each geologic province.

The work reported on here focuses on China and its surrounding regions (Figure 1). Since Pn, Lg, and Sn wave propagation characteristics are diagnostic of crust and upper mantle properties, respectively, we have examined how these waves propagate in China and its surrounding regions to better understand the active tectonics of the region and the importance of these phases for nuclear monitoring. Previously, various high-frequency waves, such as Pn, Sn and Lg, have been used to develop short-period discriminants [e.g. Pomeroy et al., 1982; Taylor et al., 1989]. For example, Pg and Lg amplitude ratios are an indication of the relative amount of compressional and shear-wave energy radiated from a seismic source. Low Pg/Lg ratios are often associated with earthquakes because their source occurs along a planar fault and radiate significant amounts of shear energy relative to compressional energy; high Pg/Lg ratios are usually associated with explosions because their source radiates more compressional than shear energy. However, these phases propagate in different parts of the earth and the regional geology along a path can alter the relative strength of the signals. This implies that a discriminant that works effectively in another geographical location will not be effective in certain regions of China. Therefore, the significance of these studies are two-fold. First, it is important to understand how the geology of a region affects Sn and Lg phase propagation and where attenuation of these phases occurs. Second, these studies can determine where the phases could be used as discriminants in China for a Comprehensive Test Ban Treaty (CTBT).

Regional Sn and Lg wave characteristics of western China
[Rapine, Ni, and Hearn, 1997]

A comprehensive study of the gross characteristics of high frequency seismic wave propagation in China and its surrounding regions was accomplished to learn more about how regional geology affects high-frequency phases and the implications for nuclear monitoring. Amplitudes of the regional seismic waves Sn and Lg relative to P coda were used to map lateral variations of shear wave attenuation in the crust and upper mantle. Over 7000 digital seismograms from 13 broadband stations of the Chinese Digital Seismic Network and Global Seismic Network (Figure 2) were visually examined in the frequency range 0.5 - 5.0 Hz. Propagation efficiencies of Sn and Lg were qualitatively analyzed by ranking their amplitudes relative to the P-wave coda. Maps showing Sn propagation raypaths with efficient, inefficient, and poor efficiencies is presented in Figures 3 to 5 and a similar set of efficiency maps for the Lg phase in Figures 6 to 8. In addition, summary maps that regionally map the propagation efficiencies for Sn and Lg are in Figures 9 and 10.

We have confirmed and refined results of previous studies by finding a lack of Sn transmission in north-central Tibet, the Ryukyu and Japan Arcs, Burma and the Baikal Rift. Efficient Sn propagation is observed in the Tien Shan, Tarim Platform, southern Tibet, Yangzi Paraplatform and Sino-Korean Platform. An important observation, which has not been previously reported, is that Sn does not propagate across Mongolia. This is similar to the northern Tibetan plateau. The elimination of Sn and the occurrence of recent volcanism in north-central Tibet and Mongolia suggest that there is partial melt in the uppermost mantle beneath those regions. In this respect, the mantle in some regions of China may be analogous to the mantle beneath the Turkish-Iranian Plateau [e.g., Kadinsky-Cade et al, 1981; Rodgers et al., 1997]. Volcanism in north-central Tibet and in the Mongolian Plateau provides evidence that the upper mantle beneath them is hot and partially melted and explains why Sn does not propagate through the regions.

High-frequency Lg waves propagate efficiently for most of China, Indochina and Mongolia. Lg signals are attenuated within central Tibet and often eliminated along its southern boundary. Crustal structure variations along with an anomalously low-Q, partially melted, crust are primarily responsible for weakened Lg amplitudes within Tibet. Propagation paths across the Sea of Japan and the Andaman Sea show blockage of the Lg phase as well when it travels across oceanic crust for more than a few hundred kilometers.

Attenuation of Coda waves in southern Tibet [Reese and Ni, 1996]

It has been demonstrated that the seismic coda for local earthquakes may be modeled as a superposition of shear waves singly scattered in a crust characterized by heterogeneities with typical size on the order of a kilometer [Aki and Chouet, 1975; Aki, 1980]. Since the waves arriving in the coda have sampled a large volume of crust and not just a single path, the seismic coda is an efficient tool for studying the average attenuation properties of the crust. Experimental estimates of elastic wave attenuation are usually described in terms of the seismic quality factor Q defined as the fractional energy loss per cycle. In general, the quality factor is a function of frequency, $Q = Q(f)$, and is a combination of intrinsic attenuation which is the loss of energy to heat and scattering attenuation that is related to the transition of coherent energy to fluctuation energy. The attenuation characteristics of the crust in the southernmost Tibetan plateau are determined from analysis of S-wave coda recorded at a temporary broadband station deployed during the 1994 INDEPTH-II experiment. A method for determining Q_c is developed which utilizes the coda spectrogram observed at a single station. In the weak single scattering approximation, the frequency dependent coda power decay, at sufficiently long lapse times, can be

written in the form,

$$P(f,t) = A g(f) |S(f)|^2 G(\beta t/2) e^{-2\pi f t / Q_c(f)}$$

where A is a constant with the dimensions of length/time, t is the lapse time, β is the shear wave velocity, $S(f)$ is the earthquake source spectrum, $G(r)$ is the geometric spreading factor, $g(f)$ is the backscattering coefficient, and $Q_c(f)$ is the dimensionless coda attenuation factor [Aki, 1980]. In deriving this equation, the source and receiver are considered coincident. This approximation is valid for times t which are large with respect to the geometric S arrival time t_s . In the high frequency regime, the functional form for $Q_c(f)$ is specified as, $Q_c(f) = \alpha(f/f_0)^b$, where f_0 is equal to 1 Hz and α is the coda quality factor at 1 Hz. The backscattering coefficient Sato [1990] in the high frequency regime may be expressed as, $g(f) = 1/a(f/f_0)^{1-b}$, where a is the typical size of medium heterogeneity. The geometric spreading term is $G(r) = (r_0/r)^2$, where r_0 is some reference distance. The frequency band of interest is postulated to lie above the earthquake source spectrum corner frequency. Under this assumption, many earthquake faulting models [e.g., Brune, 1970] yield a far-field source spectrum of the form, $S(f) = (f/f_0)^{-2}$. Substituting in, rearranging, and taking the natural logarithm of both sides yields,

$$\ln(p(f,t)t^2 f^3 f_0^{-2}) = \kappa - b \ln(f) - 2 \pi f^{1-b} f_0^b t / \alpha$$

where κ is a constant. The coda power spectrogram $P(f,t)$ is calculated for a time window beginning at some lapse time $t \gg t_s$ where t_s is the lapse time corresponding to the arrival of the S -wave. In practice the lapse time t is taken to be twice t_s . The coda quality factor $Q_c(f)$ is assumed to be independent of time throughout the time window. The function $\ln(p(f,t)t^2 f^3 f_0^{-2})$ is formed for the given frequency band. The model parameters κ , α , b are estimated by minimizing the error surface in parameter space. The error function is taken to be the F -norm of the difference between the model coda power as a function of time and the observed coda spectrogram. The minimization algorithm employs a simplex search method that does not require any error function derivative information. Although no systematic grid search is performed, convergence is robust with respect to perturbations from the starting model.

The 1994 INDEPTH-II Passive Source Experiment deployed a twelve three-component station array across the Indus-Tsangpo Suture. Nine of the stations were equipped with broadband Guralp CMG-3T seismometers with a usable frequency range of 0.01 Hz to 25 Hz. The remaining stations were equipped with Mark Products 1 Hz L-4 seismometers. The INDEPTH-II passive source experiment recorded about fifty regional earthquakes. Data were continuously recorded by Reftek 72-06 24 bit digital recorders using 50 samples per second. For this study, coda signals recorded at one of the INDEPTH-II broadband stations are used. The location of the broadband station BB05 is shown in Fig. 11. The data set consists of six earthquakes

with epicentral distances between two and four degrees. The event locations are also shown in Fig. 11.

The average S-wave coda quality factor for this continent-continent collision zone is $Q_c(f) = (160 \pm 69)(f/f_0)^{1.11 \pm 0.19}$, $1 < (f/f_0) < 4$ where $f_0 = 1$ Hz. The results are consistent with other measurements of $Q_c(f)$ in continental collisional environments which typically exhibit low values of $Q_c(f)$ at 1 Hz and a strong dependence on frequency. A comparison of $Q_c(f)$ for different regions is in Figure 12. The attenuation characteristics obtained for the Arabian-Eurasian continental collisional boundary in western Turkey are quite similar to the results reported here for the southern Tibetan plateau.

Lateral variation of Pn propagation at the CDSN station LSA

[Reese, Rapine and Ni, 1997]

Various high frequency regional phases have been used to develop short period discriminants. For example, the amplitude ratio P_n/S_n is a measure of the relative amount of compressional and shear wave energy emitted by a seismic source. Clearly, the compressional energy radiated by an explosive source is large compared to an earthquake. Thus, the ratio provides a way to discriminate explosions from earthquakes. However, the propagation efficiency of these phases is sensitive to regional geology. Thus it is important to understand the lateral variation of regional phase attenuation.

The purpose of this study is to investigate lateral variation in the attenuation of P_n phases which propagate to the CDSN station LSA from epicentral distances out to 1240 km. The data is analyzed on an event by event basis to map azimuthal changes in the apparent attenuation and correlate the variations with tectonics and surface geology. The attenuation of P_n is characterized by a constant Q model for a narrow frequency band near one Hertz.

The method for estimating lateral heterogeneities in attenuation utilizes regional spectra from events with varying distances and azimuths. The analysis assumes a simple earthquake source spectrum uniquely characterized by the moment and a frequency independent model. The displacement amplitude spectrum of a signal arriving from a source at a distance r is

$$A(f,r) = S(f) I(f) G(r) \exp[\pi f r / v_g Q] ,$$

where f is the frequency, v_g is the signal group velocity, $S(f)$ is the source spectrum, $I(f)$ is the instrument response, $G(r)$ is the geometric spreading function, and the exponential term is the effective signal attenuation characterized by the quality factor Q . The attenuation of seismic signals involves both the absorption and scattering of energy. The quality factor in this equation is the sum of two terms representing the

contributions of these two attenuation mechanisms and is sometimes called the apparent quality factor. The separation of attenuation into anelastic and scattering contributions is beyond the scope of this study. There are several effects which may affect the spectral amplitude which are not included. For instance, the site response is known to depend strongly on local geology while we have assumed it to be constant over the relatively narrow frequency bands considered. Additionally, the assumed source model spectrum does not include contributions from the radiation pattern or from source complexity. Although these effects are not explicitly included, the simple spectral amplitude representation allows a self-consistent theoretical characterization of the lateral variation in the observed spectra.

The source spectra were assumed to have a simple form with a high frequency decay of f^{-2} above the corner frequency which scales with the inverse cube root of the moment,

$$S(f) = S_0 / (1+(f/f_c)^2), \quad f_c = kv_\beta (16 \Delta\sigma / 7 M_0)^{1/3}$$

where S_0 is a constant, f_c is the corner frequency, k is a constant, v_β is the shear wave velocity at the source, $\Delta\sigma$ is the stress drop, and M_0 is the moment. The moment was estimated from the moment magnitude scale $\log M_0 = 1.5 M_w + 16.1$ with $M_w = m_b$ for the range of event magnitudes considered in this study. The constant k is equal to 0.33 for shear waves and is equal to 0.50 for compressional waves. The stress drop was assumed to be 1×10^8 dyne-cm⁻² and the shear wave velocity was taken to be the crustal average $v_\beta = 3.5$ km/sec. As in all spectral decay studies of attenuation there is a trade-off between the assumed high frequency spectral roll-off and the attenuation derived from the observed spectral decay rate. A lower source roll off would yield lower values of Q while higher spectral roll off would increase the Q estimate.

The observed displacement spectral amplitudes are corrected for instrument response and the source spectrum model. Using (1), the linear regression problem for Q is formulated as

$$\ln(D(f,r)(1+(f/f_c)^2)/I(f)) = \ln(S_0 G(r)) - \pi r f / v_g Q$$

where $D(f,r)$ is the observed spectral amplitude. The logarithm of the corrected signal spectrum is a linear function of frequency. The first term on the right hand side controls the intercept while the coefficient of f involves Q . Thus effective Q can be estimated by fitting a straight line to the observed corrected log spectrum.

The data consist of event-triggered digital seismograms recorded at the CDSN station LSA, Lhasa, Tibet, from December, 1991 to August, 1995. The data were retrieved from the Incorporated Research Institutes for Seismology-Data Management Center. The station was equipped with Streickesen Model STS-1/VBB three component systems for the broadband, long period, and very long period data. The channel used for the calculation of propagation efficiency was the broadband vertical

component BHZ. The data were digitally recorded at 20 samples per second. Event origin times, locations, and body wave magnitudes were taken from the Preliminary Determination of Epicenters catalog distributed by the U.S. Geological Survey.

Regional spectra from events with epicentral distances between 240 and 1240 km and body wave magnitudes between 4.3 and 6.1 were calculated. In general the data set provides fairly uniform azimuthal coverage. Azimuthal variations in Pn attenuation were estimated by inversion of 71 events for effective Q. The Pn spectra were computed using a fixed time window of ten seconds beginning at the onset time of the arrival. A five percent Hanning taper was applied to the signal and to a pre-event noise sample. The resulting times series were zero padded to 256 samples and Fourier transformed. The noise power spectral density was subtracted from the signal power spectral density and the displacement spectral amplitude estimated by correcting for the instrument response. The frequency band was selected on the basis of a signal to noise ratio of at least two. When the signal to noise ratio was sufficient for most of the frequency band but the signal had isolated spectral holes that fell below the noise level, a five point running average was used to smooth the signal spectrum near the spectral holes.

The spectra were corrected for the source according to (3) and Q was calculated from a straight line fit to the corrected spectra for each event. If the source calculation overcorrects the observed spectra, resulting in negative or absurdly large values for Q, the corner frequency was postulated to lie above the frequency band used in the inversion. In this case, Q is calculated by assuming that $S(f) = S_0$ over the entire frequency band considered. The errors for the model attenuation estimates were found from the data kernel and the variance of the observed spectra.

At distances greater than about 1200 km the Pn signal is attenuated below the noise floor for frequencies greater than 4 Hz. Thus, the inversion for Pn was limited to frequencies between 0.5 and 4 Hz. In these relatively narrow frequency bands, the data admit a constant Q fit. It should be noted, however, that in general Q is a function of frequency. This is especially important when trying to fit one attenuation model to data in a wide frequency band.

The apparent attenuation of Pn exhibits strong azimuthal variation. In general, the attenuation is larger for events north of the station relative to events with southerly back azimuths. The solid line is a least squares fit to a function of the form $A + B \cos \theta + C \sin \theta$, where θ is the back azimuth. These results indicate an effective attenuation of $Q_{Pn} = 240$ for northern raypaths and $Q_{Pn} = 670$ for southern raypaths.

The spatial variation in transmission efficiency to LSA for the region of study can be mapped by interpolating between the measurements of apparent quality factor. A function was fit to the observed values of Q_{Pn} using an bicubic spline grid-

ding algorithm. This method was used to map lateral variation in Pn attenuation. The results are shown in Figure 13. The event locations are shown as circles and the station is shown as a triangle. The data values were interpolated on a grid with a spacing of 1 degree. The monochrome scale is shown below the figure. The north-south, large scale variation in attenuation is clear.

Azimuthal variation of Q_{Lg} at the CDSN station LSA.

[Reese, Rapine, and Ni, 1997]

Regional tectonics play an important role in the attenuation of the crustal phase Lg. Changes in crustal thickness as well as waveguide heterogeneity and partial melt in the crust can cause significant attenuation and even blockage of Lg. In regions with complicated geology, one would expect significant lateral variation in the transmission efficiency of Lg. Because Lg is relevant for the calculation of amplitude ratios for the purposes of discrimination, it is important to understand the regional variation in Lg attenuation.

For continental paths, the regional phase Lg can be modeled successfully as the sum of higher mode surface waves or as a superposition of shear waves multiply reflected within the crustal waveguide with an approximate group velocity of 3.7 - 3.2 km/sec. The propagation of Lg is sensitive to the attenuation properties of the crust and heterogeneity of the crustal waveguide. Many studies indicate that the attenuation of Lg is correlated with tectonic setting. In terms of a quality factor Q_{Lg} , low values of Q_{Lg} near one Hertz are indicative of tectonically active areas. On the other hand, stable areas such as cratons are typically characterized by large values of Q_{Lg} at one Hertz. The quality factor is a function of frequency, $Q_{Lg} = Q_{Lg}(f)$. Areas of recent tectonism typically show strong frequency dependence of Q_{Lg} relative to stable areas. The purpose of this study is to investigate lateral variation in the attenuation of Lg which propagates to the CDSN station LSA from epicentral distances out to 1200 km. The data is analyzed on an event by event basis to map azimuthal changes in the apparent attenuation and correlate the variations with tectonics and surface geology. The attenuation of Lg is characterized by a constant Q model for a narrow frequency band near one Hertz. This method has already been described in the section on the Q for the Pn waves and the same data sources were used.

Regional spectra from events with epicentral distances between 200 and 1200 km and body wave magnitudes between 4.3 and 6.1 were calculated. In general the data set provides fairly uniform azimuthal coverage. Azimuthal variations in Lg attenuation were estimated by inversion of 93 events for effective Q. The Lg spectra were computed from seismograms with a fixed group velocity window of 3.6 - 3.0 km/sec. A fixed velocity window was chosen so that the signal contained the same

number of modes for all epicentral distances. This eliminates signal energy loss due to dispersion so that the estimated attenuation is due to absorption and scattering mechanisms only. A five percent Hanning taper was applied to the signal and to a pre-event noise sample. The resulting times series were zero padded to the nearest power of 2 and Fourier transformed. The noise power spectral density was subtracted from the signal power spectral density and the displacement spectral amplitude estimated by correcting for the instrument response. The frequency band was selected on the basis of a signal to noise ratio of at least two. When the signal to noise ratio was sufficient for most of the frequency band but the signal had isolated spectral holes that fell below the noise level, a five point running average was used to smooth the signal spectrum near the spectral holes. The spectra were corrected for the source and Q was calculated from a straight line fit to the corrected spectra for each event. If the source calculation overcorrects the observed spectra, resulting in negative or absurdly large values for Q , the corner frequency was postulated to lie above the frequency band used in the inversion. In this case, Q is calculated by assuming that $S(f) = S_0$ over the entire frequency band considered. The errors for the model attenuation estimates were found from the data kernel and the variance of the observed spectra.

The frequency band 0.5 to 3 Hz had a sufficient signal to noise ratio for all data considered. In this narrow frequency band the spectral attenuation was characterized by a constant Q model. It should be mentioned that in general Q is a function of frequency $Q=Q(f)$. This is especially relevant when fitting one self-consistent attenuation model over a wide frequency band. A least squares fit to a function of the form $A + B \cos \theta + C \sin \theta$, where θ is the back azimuth was made. The average quality factor for southern back azimuths, $90 < \theta < 270$ is $Q_{Lg} = 520$ while for northern back azimuths $Q_{Lg} = 340$. The lateral variation of Q_{Lg} can be mapped by interpolating between the measured data using a bicubic spline. The data are interpolated on a 1 degree grid and plotted in Figure 14. The circles are event epicenters and the station LSA is shown as a triangle. The monochrome scale is shown below the figure.

Conclusions

In this report we have summarized results from studies of Lg , Sn , and Pn attenuation for China and its surrounding regions. These results were obtained by students supported by this ASSERT contract.

Our investigation into Sn and Lg propagation efficiency has relevance to Comprehensive Test Ban Treaty monitoring by showing where certain regional phases will or will not propagate efficiently. High Sn attenuation makes this phase difficult to use for nuclear discrimination in most of the region examined, particularly in

northern Tibet and Mongolia. Sn remains a viable phase for Tarim platform, Sino-Korean platform and the Tien Shan. Explosions from the Lop Nor test site have Sn attenuated in all directions. Lg is attenuated at major tectonic boundaries, but could be used as a short-period nuclear discriminant in most of China as long as it is recorded within the source region. A set of summary maps showing regional propagation efficiency for Sn and Lg are included in this report as Figures 9 and 10.

The attenuation characteristics of the crust in the southernmost Tibetan plateau were further examined from analysis of coda recorded at a temporary broadband station deployed during the 1994 INDEPTH-II experiment. A method for determining Q_c is developed which utilizes the coda spectrogram observed at a single station. The average S-wave coda quality factor for this continent-continent collision zone is $Q_c(f) = (160 \pm 69)(f/f_0)^{1.11 \pm 0.19}$, $1 < (f/f_0) < 4$ where $f_0 = 1$ Hz. The results are consistent with other measurements of $Q_c(f)$ in continental collisional environments which typically exhibit low values of $Q_c(f)$ at 1 Hz and a strong dependence on frequency. In particular, the attenuation characteristics obtained for the Arabian-Eurasian continental collisional boundary in western Turkey are quite similar to the results reported here for the southern Tibetan plateau.

Attenuation in Tibet was also studied using the Pn phase. In this study, the regional scale lateral heterogeneity of Pn attenuation for a data set comprised of seismograms recorded at the CDSN station LSA from regional events with epicentral distances within eleven degrees is investigated. For the frequency band 1 to 4 Hz, the attenuation model for Pn is characterized by constant Q_{Pn} . Lateral variations in attenuation are estimated by analyzing the data on an event by event basis. Significant azimuthal variation is observed with Q_{Pn} decreasing from an average of about 670 for events south of LSA to about 240 for events north of LSA. This north-south variation is consistent with other observations indicating partially melted upper mantle beneath north central Tibet.

Finally, we made estimates of Q_{Lg} for events recorded at the CDSN station LSA, Lhasa, Tibet. The frequency band investigated was .5 to 3 Hz and a constant Q attenuation model was assumed. The results indicate that in general Q is larger for raypaths from the south to LSA relative to events north of LSA. For events north of LSA the average quality factor is $Q_{Lg} = 340$ while for southern events $Q_{Lg} = 520$.

The above Pn and Sn studies confirm that northern Tibet is underlain by mantle very near solidus temperature and southern Tibet is cooler. In addition, Lg studies suggest that northern Tibet has a mid-crust that contained partial melt. The implications for nuclear monitoring is that Sn and Lg raypaths crossing northern Tibet will not be sufficiently strong to utilize them as nuclear discriminants. This is true for events at the Lop Nor test site recorded anywhere in Tibet. In addition,

Mongolia also shows high Sn attenuation, but Lg propagates efficiently there. The Sn phase will only be of much use for events occurring in eastern China, but Lg amplitudes may be useful in most regions of China.

Acknowledgments

Jianxin Wu and Artie Rodgers have provided valuable comments throughout the course of this work. Map figures were made using GMT [Wessel and Smith, 1991].

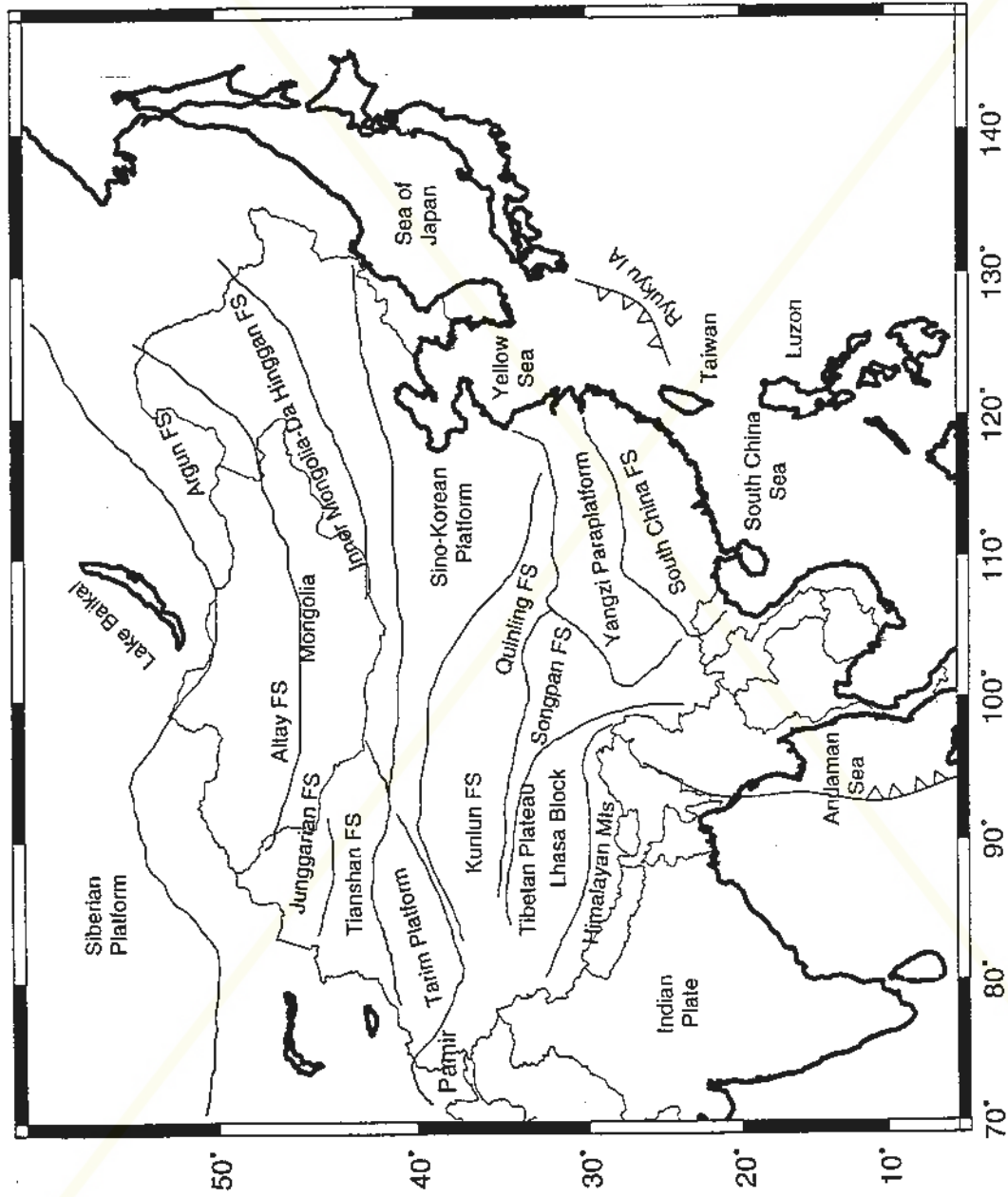


Figure 1: Tectonic map of China and surrounding regions

Commercial use is forbidden. Visit stone.abovetopsecret.com for more information on usage.

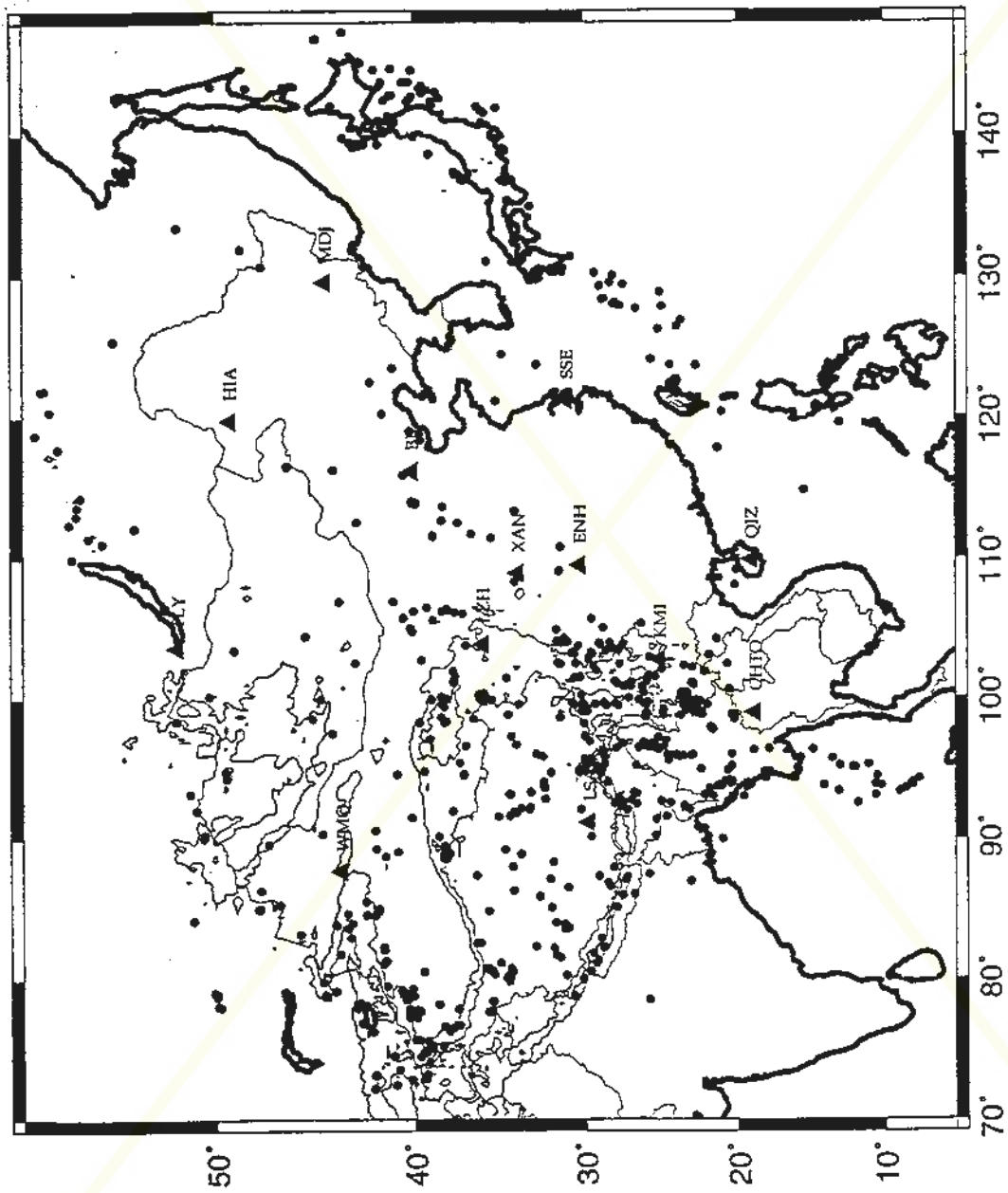


Figure 2: Map of seismic station and event locations

Commercial use is forbidden. Visit stone.abovetopsecret.com for more information on usage.

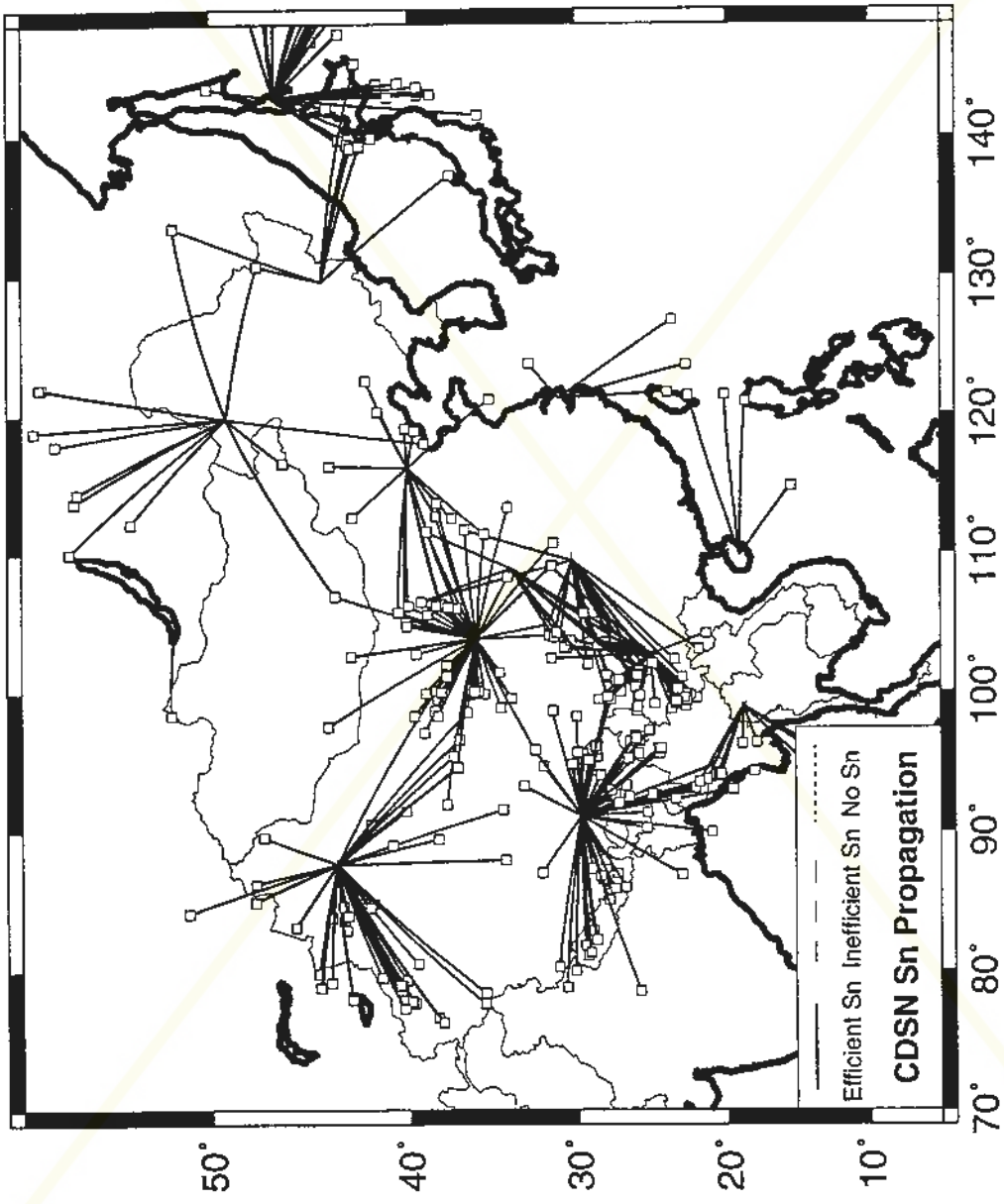


Figure 3: Map of efficient Sn propagation paths in China

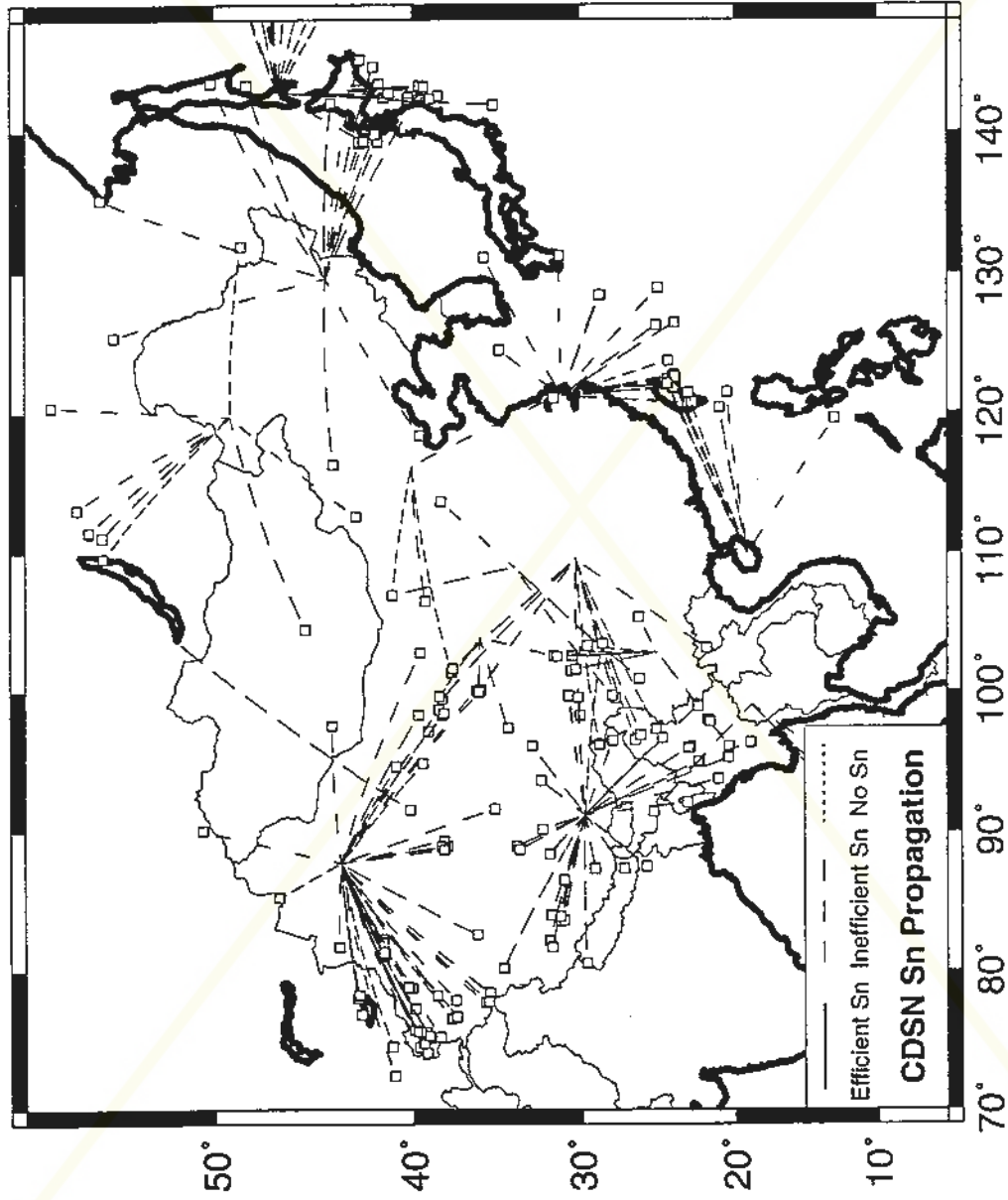


Figure 4: Map of inefficient Sn propagation paths in China

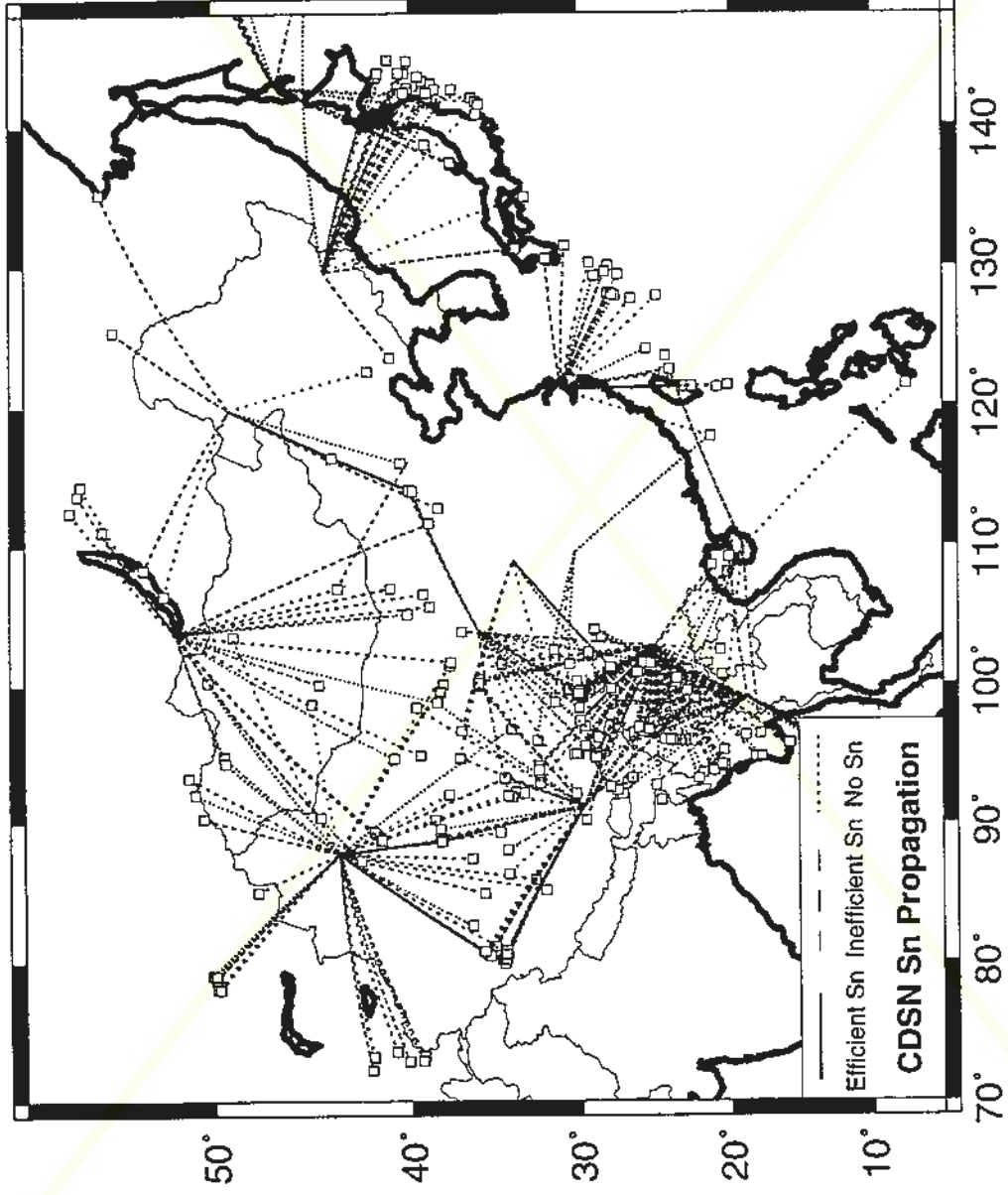


Figure 5: Map of poor Sn propagation paths in China

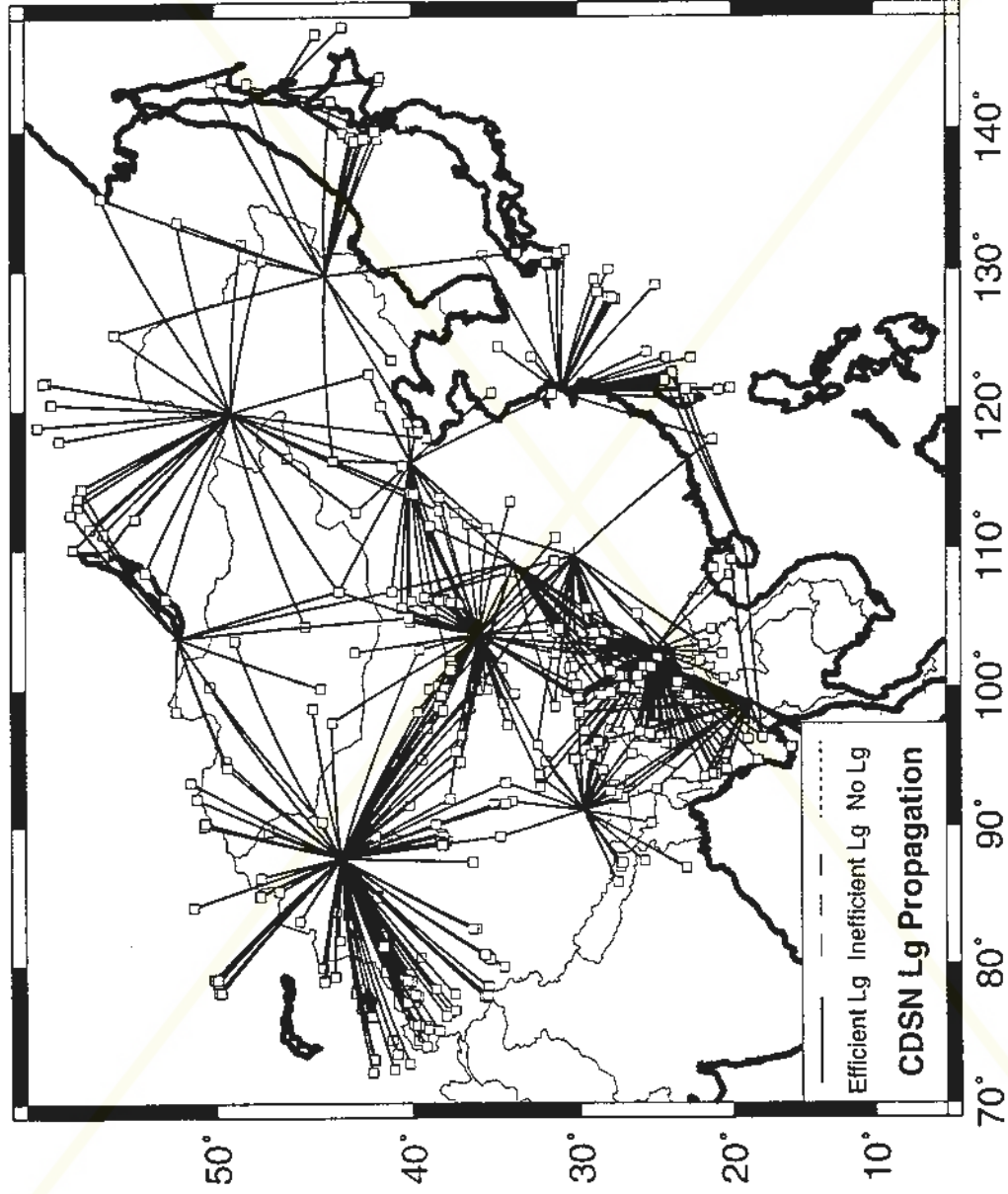


Figure 6: Map of efficient Lg propagation paths in China

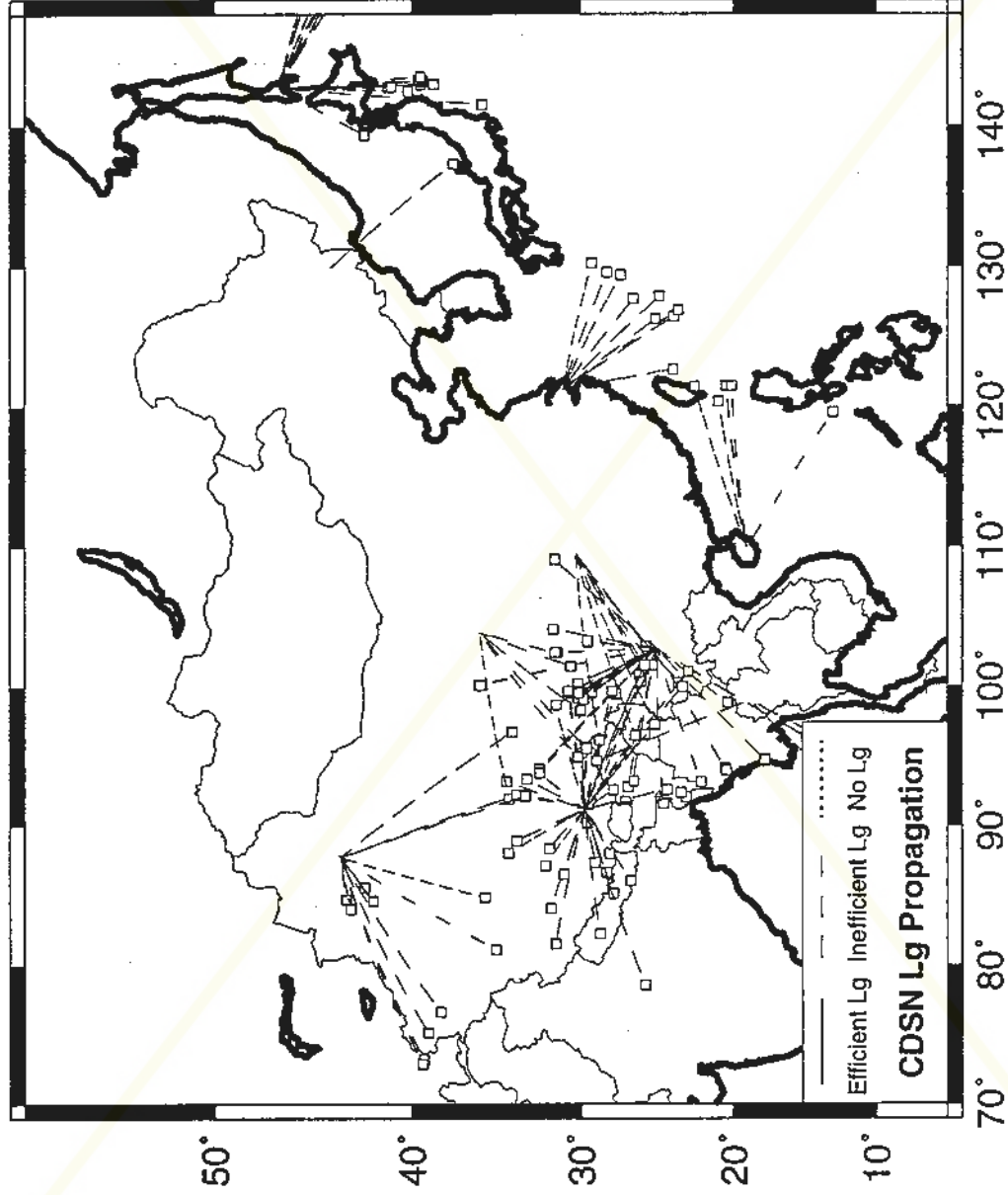


Figure 7: Map of inefficient Lg propagation paths in China

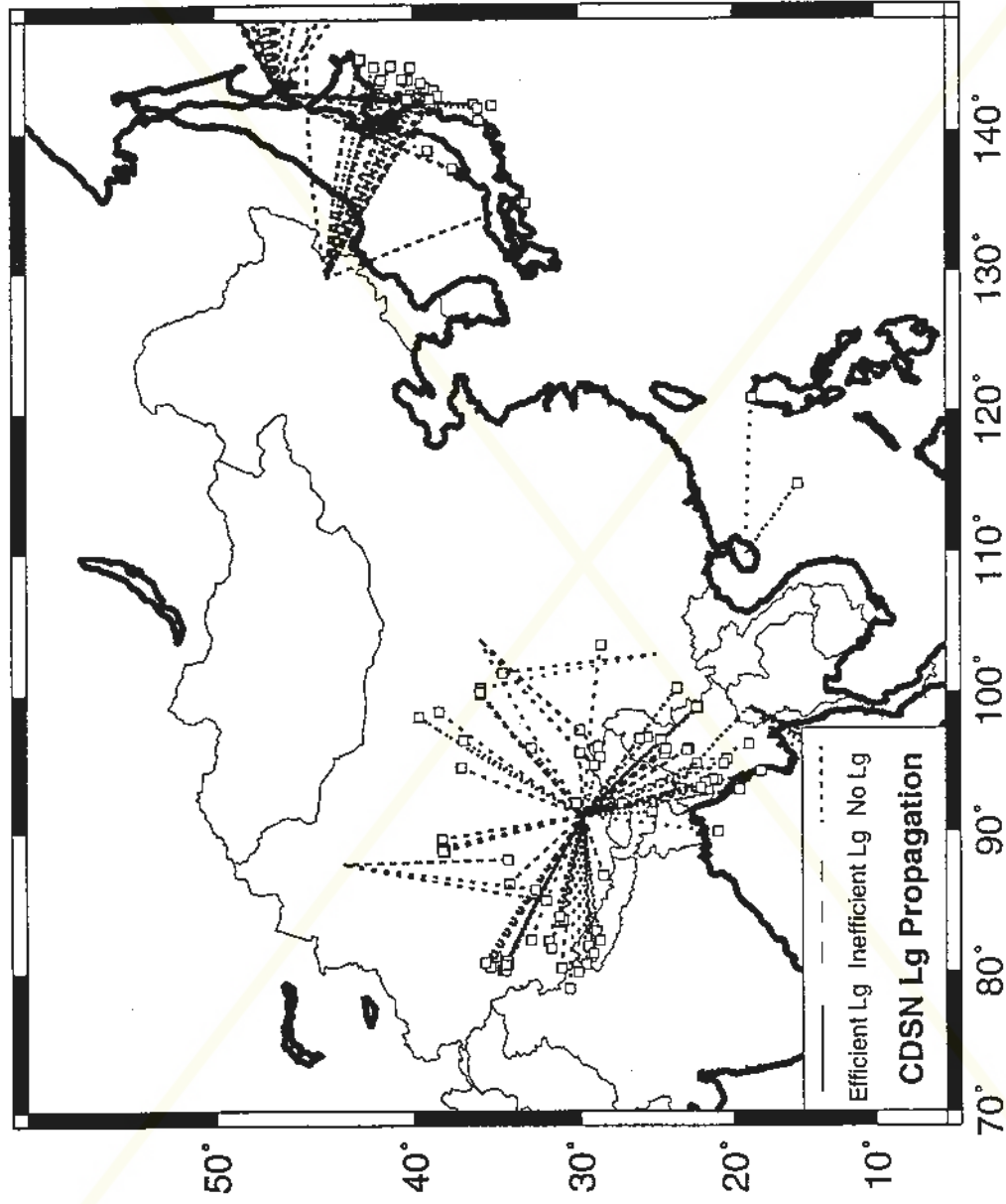


Figure 8: Map of poor Lg propagation paths in China

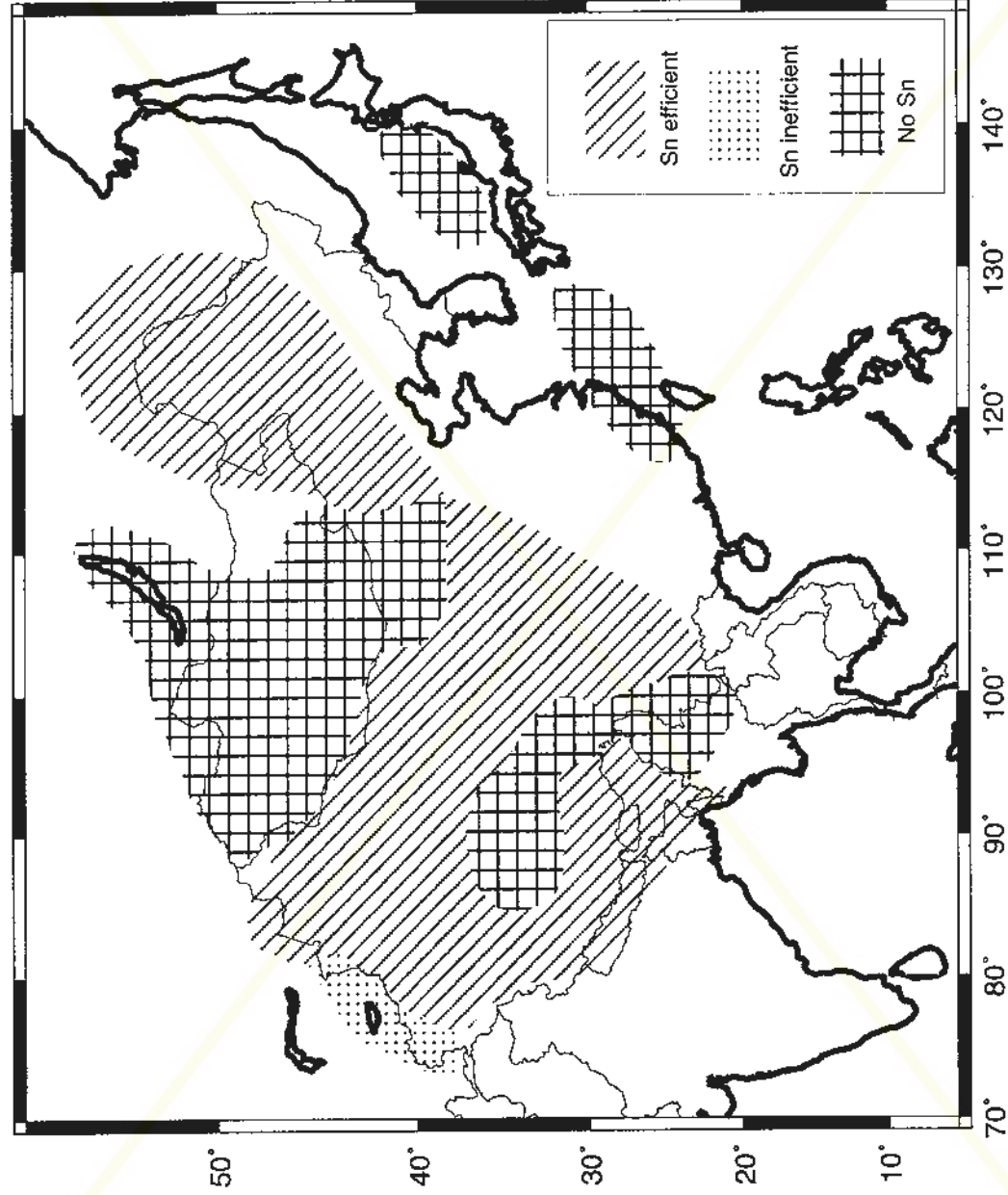


Figure 9. Summary map of Sn propagation in China

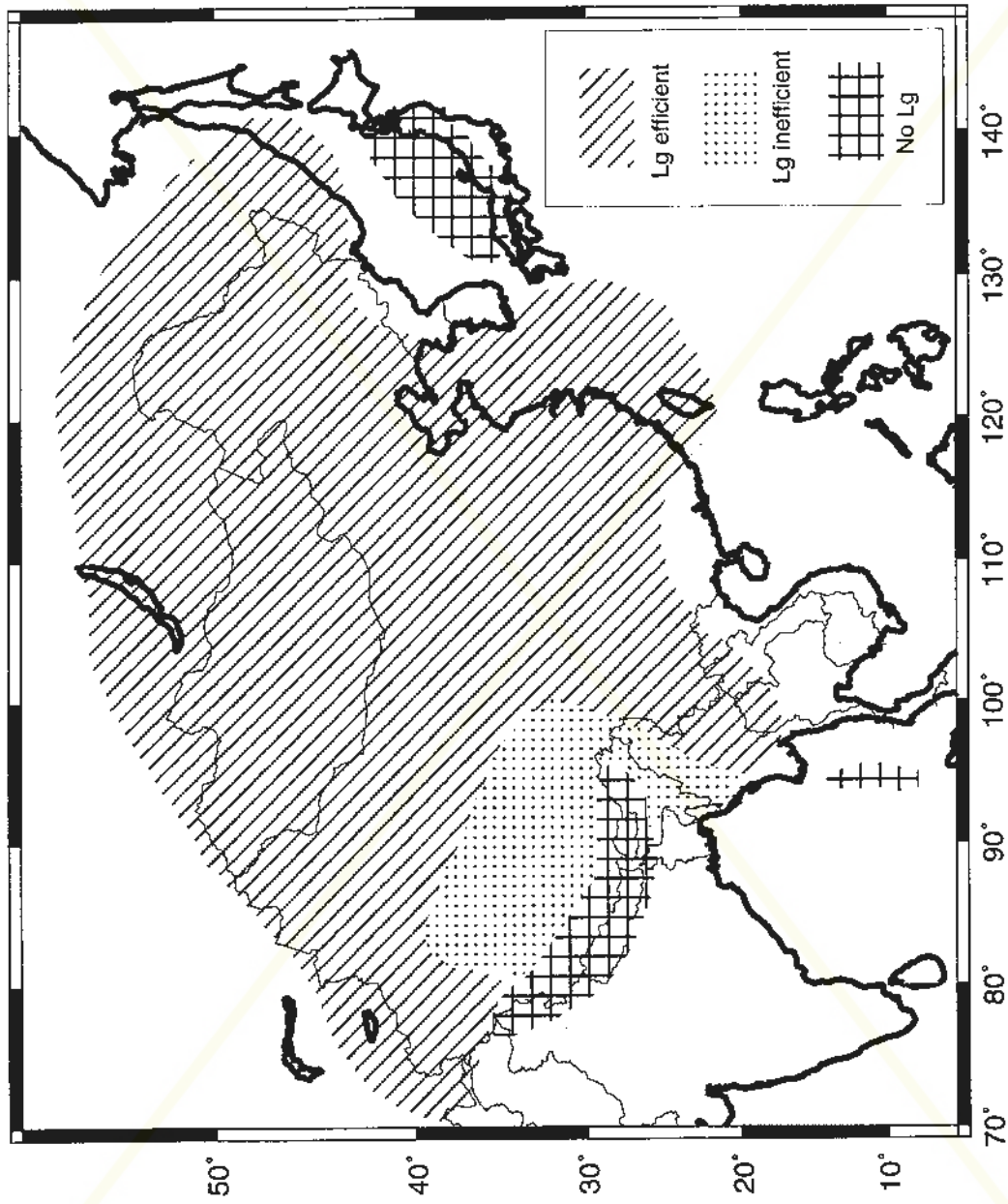


Figure 10. Summary map of Lg propagation in China

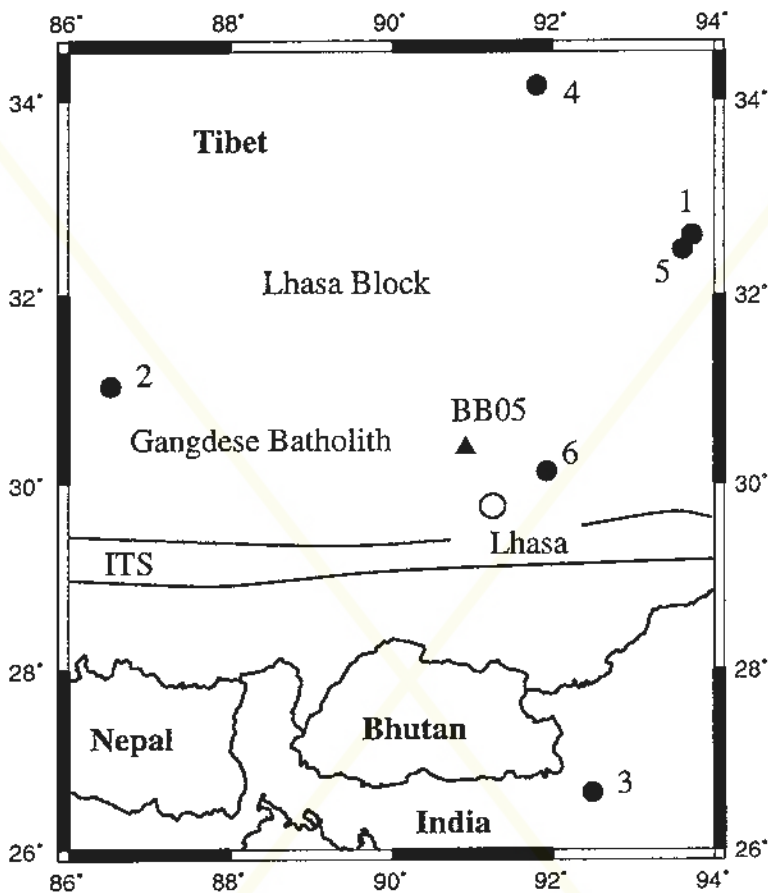


Figure 11: Station and event location map for Tibet

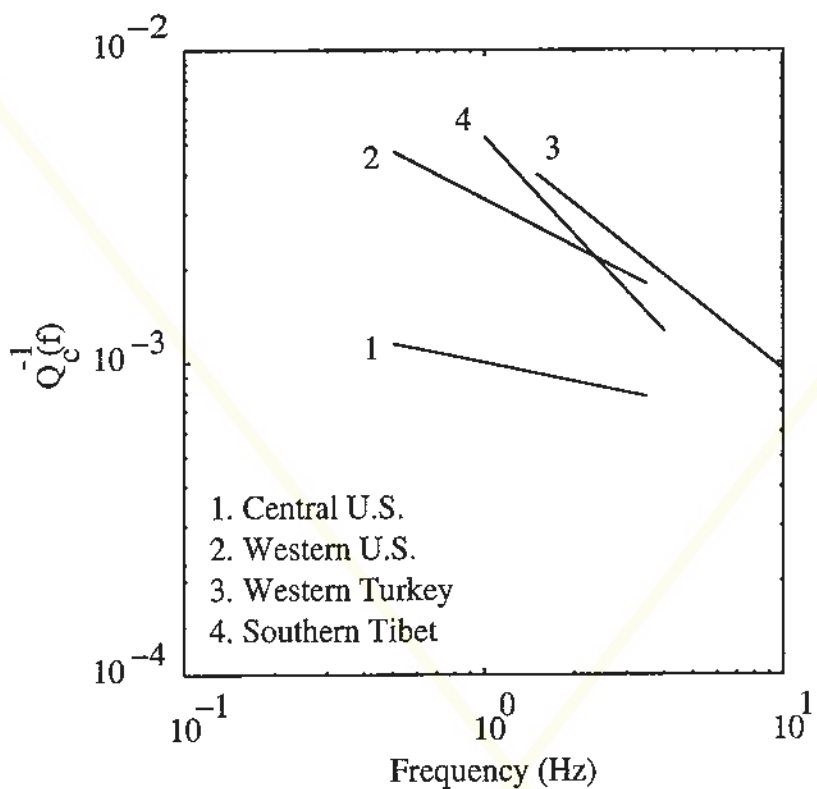


Figure 12. Comparison of coda Q for different regions.

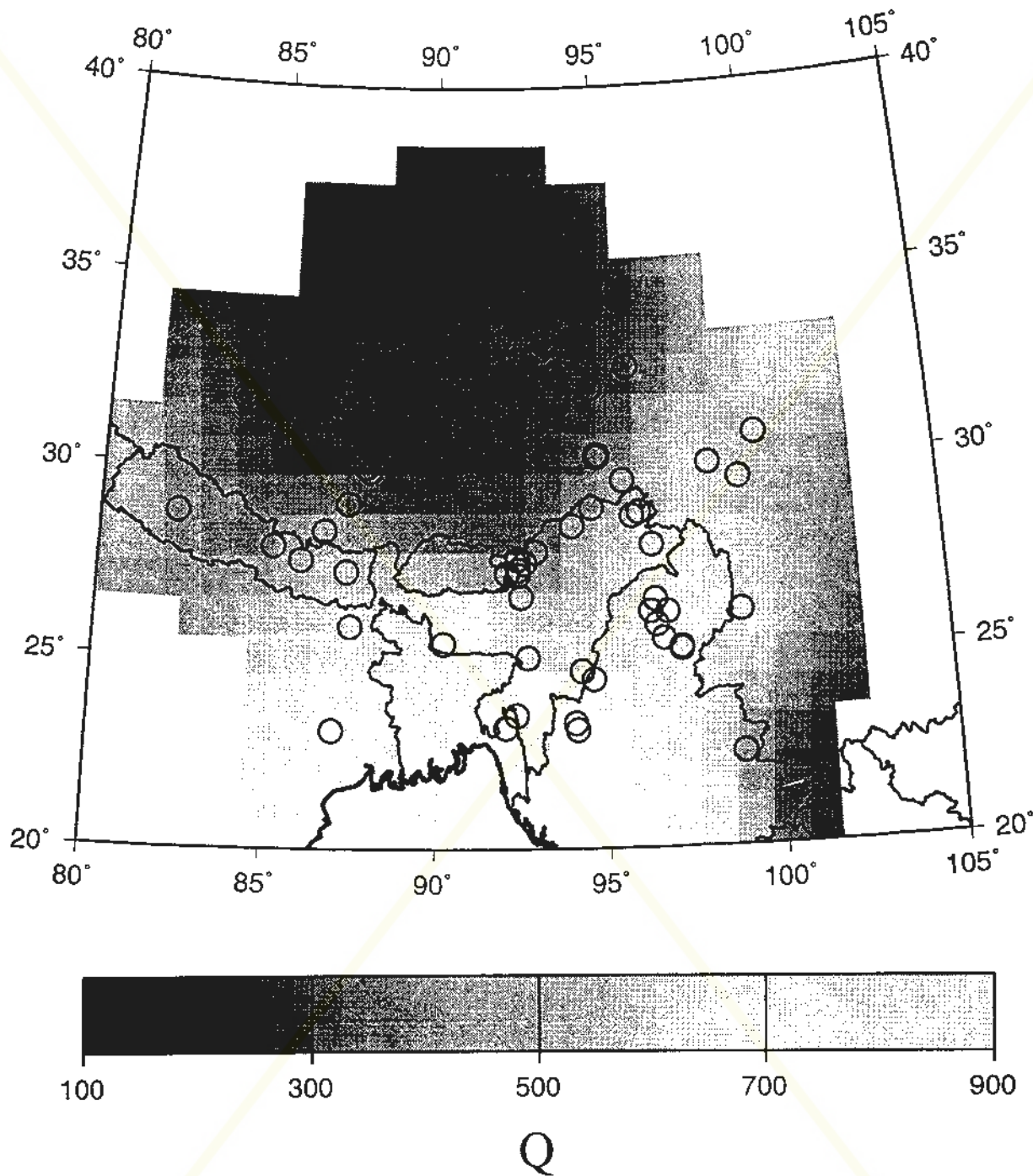


Figure 13. Map of Pn Q for Tibet from station LSA

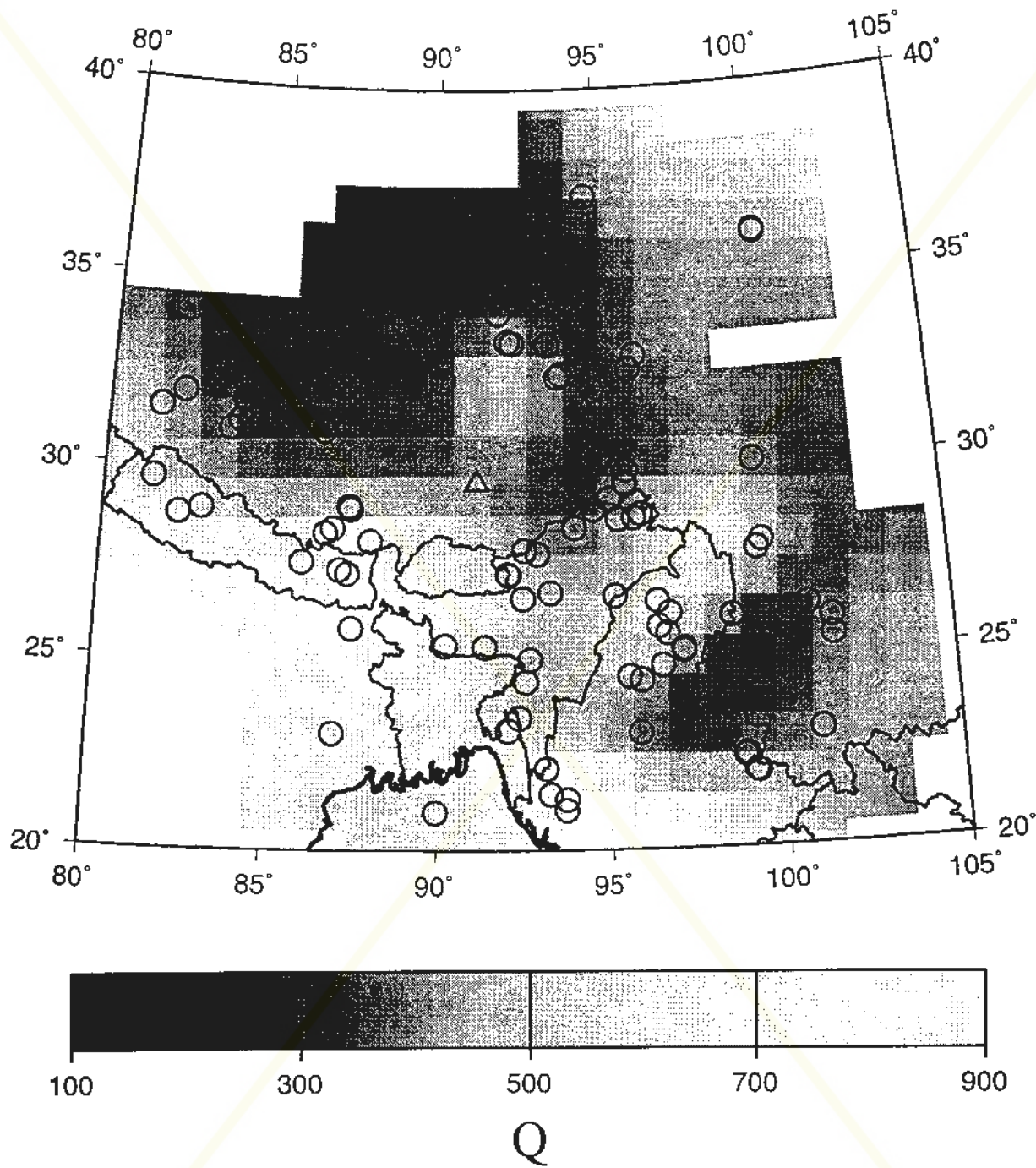


Figure 14. Map of Lg Q for Tibet from station LSA

References

- Aki, K. and B. Chouet, Origin of Coda Waves: Source, Attenuation, and Scattering Effects, *J. Geophys. Res.*, 80, 3322-3342, 1975.
- Aki, K., Scattering and Attenuation of Shear Waves in the Lithosphere, *J. Geophys. Res.*, 85, 6496-6504, 1980.
- Akinci, A., A.G. Taktak, and S. Ergintav, Attenuation of Coda Waves in Western Anatolia, *Phys. Earth Plan. Int.*, 87, 155-165, 1994.
- Brune, J.N., Tectonic Stress and the Spectra of Seismic Shear Waves from Earthquakes, *J. Geophys. Res.*, 75, 4997-5002, 1970.
- Chinese Academy of Geological Sciences, Map of tectonic systems of the People's Republic of China (in Chinese), Cartographic Publishing House, Beijing, 1:4,000,000, 1976.
- Coleman, R. G., Continental growth of northwest China, *Tectonics*, 8, 621-635, 1989.
- Hearn, T., and J. Ni, Pn Tomography of Southern Europe from Pn Data, *EOS Trans Am Geophys Union*, 72, number 44, page 349, presented at the December 1991 American Geophysical Union Meeting, 1991.
- Hearn, T., and J. Ni, Pn Travel-Time Tomography of Eurasia, *Seismological Research Letters*, v63, n1, p27, 1992a.
- Hearn, T., and J. Ni, Low Pn Velocity and the Turkish-Iran Plateau, *EOS Trans Am Geophys Union*, v73, n14, p209, April 1992b.
- Hearn, T., and J. Ni, Low Uppermost Mantle Velocity Beneath the Western Hindu-Kush Range, *EOS Trans. Am. Geophys. Union*, v73, n43, p408, Oct. 27, 1992c.
- Hearn, T., and J. Ni., Pn velocities beneath continental collision zones: the Turkish-Iranian Plateau, *Geophys. J. Int.*, 117, 273-283, 1994.
- Hearn, T. and J. Wu, Pn Anisotropy beneath Southern Europe, *EOS Trans. AGU*, 76, 46, pF413, 1995.
- Hearn, T. and J. Wu, Anisotropic Pn Tomography beneath Southern Europe, in preparation for *Geophysical Journal International*, 1996.
- Huang, J., Tectonic map of China, scale 1:4,000,000 (in Chinese), Cartographic Publishing House, Beijing, 1979.
- Huang, J., R. Jishuan, J. Chunfa, Z. Zhengkun, and Q. Deyu, Geotectonic evolution of China, Science Press, Beijing, and Springer-Verlag, Berlin, 214 p., 1987.
- Kadinsky-Cade, K., M. Barazangi, J. Oliver and B. Isacks, Lateral variations in high-frequency seismic wave propagation at regional distances across the Turkish and Iranian Plateaus, *J. Geophys. Res.*, 86, 9377-9396, 1981.
- Ni, J., R. Rapine, J. Wu, and T. Hearn, Regional wave propagation characteristics in China and southern Asia, *17th Annual Seismic Research Symposium*, Sept. 11-15, Scottsdale, Az., 1995.

- Pomeroy, P. W., W. J. Best, and T. V. McEvelly, Test ban treaty verification with regional data - a review, *Bull. Seism. Soc. Am.*, 72, S89-S129, 1982.
- Rapine, R., J. Wu, J. Ni, T. Hearn, Regional Sn and Lg wave propagation efficiencies in China, Indochina, and Mongolia, *EOS Trans. AGU*, 76, 46, pF428, 1995.
- Reese, C., J. Ni and T. Hearn, Scattering attenuation in fractally homogeneous random media, *17th Annual Seismic Research Symposium*, Sept. 11-15, Scottsdale, Az, 1995.
- Reese, C.C. and J.F. Ni, Attenuation of coda waves in souther Tibet, *Geophys. Res. Lett.*, 23,3015-3019, 1996
- Reese C., R. Rapine and J. Ni, Lateral Variation of Pn and Lg Propagation at the CDSN Station LSA, in preparation for *Bull. Seism. Soc. Am.*, 1997.
- Rodgers, A., T. Hearn, and J. Ni, July 1994. Uppermost Mantle Structure in Southern Eurasia from Pn Tomography and Sn Attenuation, paper for the *16th Annual Seismic Research Symposium*, Thornewood, NY, September 1994a.
- Rodgers, A., T. Hearn, and J. Ni, Pn, Sn, and Lg Propagation in the Middle East, *EOS Trans Am Geophys Union*, 75, 463, presented at the December, 1994 American Geophysical Union Meeting, San Francisco, CA, 1994b.
- Rodgers, A., J. Ni, and T. Hearn, Propagation characteristics of short period Sn and Lg in the Middle East, *Bulletin of the Seismological Society of America*, 87, 396-413, 1997.
- Singh, S.K. and R.B. Herrmann, Regionalization of Crustal Coda Q in the Continental United States, *J. Geophys. Res.*, 88, 527-538, 1983.
- Sato, H., Energy Propagation Including Scattering Effects: Single Isotropic Scattering Approximation, *J. Phys. Earth*, 25, 27-41, 1977.
- Taylor S. R., M. D. Denny, E. S. Vergino, and R. E. Glaser, Regional discrimination between NTS explosions and earthquakes, *Bull. Seism. Soc. Am.*, 79, 1142-1176, 1989.
- Wessel, P. and Smith, W., Free software helps display data, *EOS Trans. Amer. Geophys. U.* 72, 441, 445-446, 1991.
- Wu, J., J. Ni, and T. Hearn, Lg wave attenuation and propagation characteristics in Iran, in *Monitoring a Comprehensive Test Ban Treaty*, NATO ASI Volume, Eds., E. Husebye and A. Dainty, 655-662, Kluwer Academic Publishers, 1996.

Publications with support from this contract and its companion contracts

Reviewed publications

- Hearn, T. and J. Wu, Anisotropic Pn Tomography beneath Southern Europe, submitted to *Geophysical Journal International*, 1997.
- Rapine, R., J. Ni, J. Wu, and T. Hearn, Wave propagation in China and surrounding regions, *Bulletin of the Seismological Society of America*, in press, Dec. 1997.
- Reese, C.C. and J.F. Ni, Attenuation of coda waves in southern Tibet, *Geophys. Res. Lett.*, 23,3015-3019, 1996
- Reese, Rapine and Ni, Lateral Variation of Pn and Lg Propagation at the CDSN Station LSA, in preparation for *Bull. Seism. Soc. Am.*, 1997.
- Rodgers, A., J. Ni, and T. Hearn, Propagation characteristics of short period Sn and Lg in the Middle East, *Bulletin of the Seismological Society of America*, 87, 396-413, 1997.
- Wu, Jianxin, J. Ni, and T. Hearn, Lg wave attenuation and propagation characteristics in Iran, in *Monitoring a Comprehensive Test Ban Treaty*, NATO ASI Volume, Eds., E. Husebye and A. Dainty, 655-662, Kluwer Academic Publishers, 1996.
- Hearn, T., and J. Ni, Pn velocities beneath continental collision zones: The Turkish-Iranian Plateau, *Geophys. J. Int.*, 117, 273-283, 1994.

Conference proceedings

- Rapine, R., T. Hearn, J. Wu, and J. Ni, Sn and Lg propagation characteristics beneath China, in *Proceedings of the 18th Annual Seismic Research Symposium on Monitoring a Comprehensive Test Ban Treaty*, 4-6 September 1996, 88-97, 1996.
- Rapine, R., J. Ni, and T. Hearn, Wave propagation in China and surrounding regions, *Proceedings of the 19th Annual Symposium on Monitoring a CTBT*, 135-142, Orlando, FL., 1997.
- Reese, C., J. Ni and T. Hearn, Scattering attenuation in fractally homogeneous Random media, *17th Annual Seismic Research Symposium*, Sept. 11-15, Scottsdale, Az, 1995.
- Rodgers, A., T. Hearn, and J. Ni, July 1994. Uppermost Mantle Structure in Southern Eurasia from Pn Tomography and Sn Attenuation, paper for the *16th Annual Seismic Research Symposium*, Thornewood, NY, September 1994.
- Ni, J., R. Rapine, J. Wu, and T. Hearn, Regional wave propagation characteristics in China and southern Asia, *17th Annual Seismic Research Symposium*, Sept. 11-15, Scottsdale, Az., 1995.

Ni, J., C. Reese, J. Wu, and L-S Zhao, Crustal structure and attenuation in Southern Tibet, in *Proceedings of the 18th Annual Seismic Research Symposium on Monitoring a Comprehensive Test Ban Treaty*, 4-6 September 1996, 390-399, 1996.

Meeting abstracts presented

Hearn, T., and J. Ni, Pn Tomography of Southern Europe from Pn Data, *EOS Trans Am Geophys Union*, vol 72, number 44, page 349, presented at the December 1991 American Geophysical Union Meeting.

Hearn, T., and J. Ni, Low Pn Velocity and the Turkish-Iran Plateau, *EOS Trans Am Geophys Union*, v73, n14, p209, April 1992, presented at the 1992 Spring American Geophysical Union Meeting, May 1992, Montreal, Canada.

Hearn, T., and J. Ni, Pn Travel-Time Tomography of Eurasia, *Seismological Research Letters*, v63, n1, p27, 1992, presented at the April 1992 Seismological Society of America Meeting, Santa Fe, New Mexico.

Hearn, T., and J. Ni, Low Uppermost Mantle Velocity Beneath the Western Hindu-Kush Range, *EOS Trans Am Geophys Union*, v73, n43, p408, Oct. 27 1992, presented at the 1992 Fall American Geophysical Union Meeting, December 1992, San Francisco, CA.

Hearn, T. Anisotropic Tomography beneath the Western U.S., presented at the Seventh Annual IRIS Workshop, Jackson Hole, WY 1995.

Hearn, T. and J. Wu, Pn Anisotropy beneath Southern Europe, *EOS Trans. Am. Geophys. Union*, 76, 46, pF413, 1995.

Mele, G., M. Barazangi, T. Hearn, A. Rovelli, and D. Seber, High-frequency Seismic Wave Propagation in the Uppermost Mantle beneath Italy, *International Union of Geodesy and Geophysics XXI General Assembly*, July 2-14, 1995.

Rapine, R., J. Wu, J. Ni, T. Hearn, Regional Sn and Lg wave propagation efficiencies in China, Indochina, and Mongolia, *EOS Trans. AGU*, 76, 46, pF428, 1995.

Rapine, R., J. Ni, T. Hearn, Sn and Lg attenuation and regional propagation characteristics in China, *EOS Transactions, AGU*, November 1996.

Rodgers, A., T. Hearn, and J. Ni, Pn, Sn, and Lg Propagation in the Middle East, *EOS Trans Am Geophys Union*, 75, 463, 1994

Wu, J., J. Ni, and T. Hearn, Lg Wave Attenuation and Propagation Characteristics in Iran, *Seismological Research Letters*, 66, 2, 51, 1995.

Personnel

Principle Investigators:

- Thomas M. Hearn, Assistant Professor, Physics Dept., New Mexico State University. Geophysics Ph.D. Caltech 1985, Geophysics, Thesis: Crustal Structure in Southern California from Array Data. Geophysics M.S. Caltech 1982.
- James F. Ni, Professor, Earth Sciences Ph.D. Cornell, 1984, Thesis: Seismicity and Active Tectonics of the Himalayas and Tibet. Civil and Environmental Engineering M. Engr. 1973.

Graduate Students and Postdoctoral Associates:

- Richard Rapine, Graduate Student, Physics Dept., New Mexico State University.
- Chris Reese, Graduate Student, Physics Dept., New Mexico State University.
- Arthur Rodgers, Postdoctoral Associate, Physics Dept., New Mexico State University. Physics, 1994. Ph.D. University of Colorado 1993, Thesis: Tomographic Imaging of Internal Earth Structure: The Core-Mantle boundary and the Trade-off between Volumetric and Topographic Structure. Physics M.S. 1988. Now at University of California at Santa Cruz, Department of Earth Sciences.
- Jianxin Wu, Graduate Student / Postdoctoral Associate, Physics dept., New Mexico State University. Ph.D., New Mexico State University, 1995.

Figure Captions

- Figure 1. A simplified tectonic map of China and its surrounding regions. Dark lines separate the major tectonic provinces in the region. Triangles represent the direction of oceanic subduction. (FS-Fold System, IA-Island Arc, Mts-Mountains) (modified from Huang et al., 1987; Huang, 1979; Coleman, 1989; Chinese Academy of Geological Sciences, 1976)
- Figure 2. A station map for the Chinese Digital Seismic Network (CDSN) stations we investigated. Black triangles represent station locations. Black dots are event locations used in this study. Gray lines represent 2000 and 4000 m elevation contours. There are two Global Seismic Network (GSN) stations we have also included - TLY (Lake Baikal) and CHTO (Thailand).
- Figure 3. A map of efficient Sn propagation paths in China. The squares represent seismic events. The solid lines depict efficient station-event paths in the regions of study. All paths have epicentral distances between 2 degrees and 15 degrees and all events are less than 50 km deep and have body wave magnitudes greater than 4.3. Capital letters represent locations of the earthquakes depicted on seismograms from Figures 3 and 4 and discussed in the text.
- Figure 4. A map of inefficient Sn propagation paths in China. Dashed lines represent inefficient station-event paths.
- Figure 5. A map depicting the station-event paths where no Sn phase was observed or where Sn was severely attenuated. For this case, propagation paths are represented by dotted lines.
- Figure 6. A map of efficient Lg propagation paths in China. Solid lines depict efficient Lg ray paths.
- Figure 7. A map of inefficient Lg propagation paths in China. Dashed lines represent inefficient station-event paths.
- Figure 8. A map depicting the propagation paths where Lg was completely eliminated or severely attenuated in China. Paths of Lg blockage are depicted by dotted lines.
- Figure 9. This is a summary map depicting the approximate regions of efficient, inefficient and no Sn propagation in the area of study. These are based on gross characteristics and are not definitive boundaries. Figure 10. A summary map for efficient, inefficient and no Lg propagation in China and its surrounding regions.
- Figure 11. A map showing the location of the INDEPTH-II broadband station BB05 and the epicenters of the events used for this study. The station location is shown as a triangle and event locations as circles. The event numbers correspond to Table 1. The area covered by the INDEPTH-II array extends from the northern edge of

the High Himalaya, through the Indus-Tsangpo suture, to the southern Tibetan plateau.

Figure 12. The results of some previous estimates of $Q_c(f)$ and the results of this study demonstrate the correlation with tectonic province. Low values of $Q_c(f)$ at one Hertz and a strong frequency dependence are indicative of tectonically active areas. The results for the United States are from Singh and Hermann, (1983) while the Western Turkey value is from the work of Akinici et. al., (1994). The results for Southern Tibet and Western Turkey are quite similar with values of about 150-200 for Q_c at 1 Hz measured at a 200 sec. lapse time.

Figure 13. A map of Q_{Pn} interpolated on a square grid of 1 degree spacing. The events are shown as circles and the station LSA is shown as a triangle. A bicubic spline algorithm was used for the interpolation.

Figure 14. A map of Q_{Lg} interpolated on a grid of 1 degree spacing. The events are shown as circles and the station LSA is shown as a triangle. A bicubic spline algorithm was used for the interpolation.